Powder Technology 449 (2025) 120419

Contents lists available at ScienceDirect

Powder Technology

journal homepage: www.journals.elsevier.com/powder-technology

Systematic analysis of mixing and segregation patterns of binary mixtures in fluidised beds for multi-functional processes

Hualun Zhu, Paola Lettieri, Massimiliano Materazzi *

Department of Chemical Engineering, University College London, London WC1E 7JE, UK

HIGHLIGHTS

- The study explores mixing and segregation of Geldart Group A and B powders in binary systems.
- Modified Cheung and Gibilaro-Rowe models are used to analyze segregation behaviours.
- Real-time mixing and segregation are analyzed using novel non-invasive X-ray imaging.
- Findings support the design and optimization of thermochemical conversion technologies.

GRAPHICAL ABSTRACT

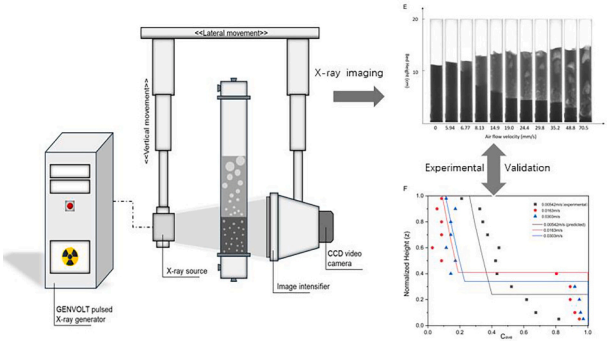

ARTICLE INFO

Keywords:
Binary particles
X-ray imaging
Fluidized bed
Mixing and segregation
Sorption-enhanced

ABSTRACT

Fluidized beds are increasingly used in renewable energy and chemical production due to their versatility in handling different solids for multi-functional industrial applications. The diversity in size and density of solid particles impacts fluidization, influencing mixing and segregation behaviours critical for optimizing chemical processes and reactor design. This study investigates the expansion and segregation behaviours of mixed Geldart group powders in binary systems, simulating polydispersed beds with different materials and catalysts. By applying a modified Cheung equation and an adapted Gibilaro-Rowe model, the study analyzes segregation behaviours of Geldart Group A and B materials at varying mixing rates and gas flow velocities. Results show a good match between experimental data and model predictions. Using novel non-invasive X-ray imaging, the study provides real-time analysis of mixing and segregation at different fluidization regimes and temperatures. These findings aid in designing and optimizing advanced thermochemical conversion technologies, enhancing process efficiency and resilience.

1. Introduction

Fluidized bed technology is increasingly recognized as a highly efficient and versatile method with wide-ranging applications in the arenas of sustainable energy and manufacturing [1,2]. This technology has become particularly relevant in diverse industrial applications where the concurrent handling of different solid materials is crucial [3]. These applications encompass enhanced sorption catalysis/synthesis

* Corresponding author.
E-mail address: massimiliano.materazzi.09@ucl.ac.uk (M. Materazzi).

https://doi.org/10.1016/j.powtec.2024.120419
Received 5 August 2024; Received in revised form 23 October 2024; Accepted 1 November 2024
Available online 2 November 2024

[4,5], upgrading of synthetic crude oil [6,7], chemical looping [8,9], and others [10,11].

The core concept behind fluidized beds is based on suspending solid particles within a fluid medium, either liquid or gas, which enables dynamic and effective interactions between the solid and gaseous phases [12]. These systems are characterized by the presence of particles of varying sizes and densities, which lead to segregation at certain gas velocity ranges [13]. The distribution and homogeneity of these particles significantly influence the bed's performance in aspects such as flow patterns, heat transfer, and chemical reactions.

A common design in fluidized bed systems is the dual fluidized bed configuration, which consists of a catalytic and a regeneration reactors [14]. This arrangement utilizes two separate vessels, each designated for a specific function within the process [14,15]. The catalytic reactor facilitates the desired chemical reactions or transformations, often involving catalytic activities on different solid phases, whereas the regeneration reactor focuses on renewing the reactivity and functionality of one type (or more) of solids involved in the reaction. For example, sorption-enhanced methanation uses CaO-based sorbents or spherical 3 A zeolite to capture H_2O in situ, promoting CH_4 production on normal Nickel-based catalysts. The reacted sorbents are then transported to a calciner, where a higher temperature is applied for dehydration, and the regenerated CaO/zeolite is subsequently recycled back into the methanator [16,17]. In the context of dual fluidized bed systems, it is imperative to note that typically only one type of solid material (e.g. the sorbent) is circulated between the two reactors, in order to avoid thermal and redox stress to the metal catalyst [15,18]. This circulatory mechanism is fundamental to the system's efficient and continuous operation, and significantly augments the sustainability and economic viability of these operations by minimizing the necessity for continual replenishment of solid materials and by maximizing their utility [19,20].

In these industrial applications, multi-functional powders have typically varied densities and size distributions [21]. The bed's hydrodynamics are markedly affected by minor variations in these parameters. For example, changes in the average size of the particle mixture due to alterations in particle size distribution can significantly impact the bed's behaviour [22]. A mixture comprising the same type of particles but with different average sizes will exhibit a minimum fluidization velocity that falls between the minimum fluidization velocities of the individual particle sizes [23]. The mixing states of binary systems in fluidized beds can be categorized into complete mixing, complete segregation, and partial mixing, each affecting the system's efficiency and effectiveness in distinct ways.

Segregation of particles refers to the process by which particles of different types, sizes, or densities separate from a mixture, leading to a non-uniform distribution [24]. This phenomenon can be observed in various industries and natural processes. Segregation can occur due to a variety of mechanisms. Understanding the mechanisms of particle segregation is crucial for industries, and especially for multifunctional systems whose design relies on the different behaviour of the solid phases [25]. Gibilaro and Rowe's two-phase GR model, developed in 1974, describes the dynamics within segregating fluidized beds by distinguishing between the wake phase, where solids ascend with bubbles, and the bulk phase, which contains the remaining solids [26]. The model incorporates three mixing mechanisms—circulation, exchange, and axial mixing—and a segregation mechanism influenced by the physical properties of the solids, such as density and size. This leads to different segregation patterns depending on these properties.

The recent published work on the behaviour of fluidized beds predominantly focuses on gas-solid fluidized beds. While there are some studies centred on CFD modelling of binary particle systems [27,28], accurately determining the conditions that govern transitions between mixing and segregation states remains a significant challenge [29], as conventional methods often fail to capture the complex interactions within the different solid phases. Additionally, predicting behaviour across different mixtures using software is complex and requires substantial time and computational effort. To address this, our study uses real-time X-ray imaging to capture more accurate particle dynamics, helping to characterizing the transition conditions and improve predictive model.

This study aims to provide an alternative solution that simplifies the prediction and understanding of mixing and segregation behaviour in multi-functional fluidised beds and compares these predictions with experimental results. In our study, we applied a modified Gibilaro and Rowe (GR) model that de-emphasizes the impact of axial mixing [30]. Additionally, we introduced a modified Cheung equation (Fu et al. equation) [31,32] to estimate the minimum fluidization velocity of binary systems. By combining these correlations, we aimed to obtain results that better support the model's predictions. We analyzed the effects of gas velocities and jetsam proportions on mixing and segregation behaviours, effectively characterizing solid concentration profiles across varied conditions. Deploying the improved models simplifies the prediction and modelling of these behaviours, enhancing efficiency and performance in multi-functional reactor and process design.

2. Materials and experimental

The structural design of the reactor, as depicted in Fig. 1, consists of a 2 mm thick Perspex cylinder with a diameter of 28 mm and a height of 530 mm. A crucial element for achieving efficient fluidization is the integration of a precision engineered Hastelloy X distributor plate. This plate, characterized by its 40 μm porosity, is specifically designed to create a significant pressure drop, thereby optimizing fluidization conditions within the reactor.

Positioned directly below the distributor plate is a wind box, constructed from stainless steel and measuring 25 mm in height. This section is densely packed with 5 mm diameter ceramic balls, arranged with the aim of ensuring uniform gas distribution across the reactor. The reactor's upper section is closed with a stainless-steel mesh lid. Attached to this lid is a hose pipe that performs the dual functions of providing pressure relief and capturing elutriated particles. This hose extends to a cylindrical beaker, which is 170 mm tall and 15 mm in diameter, filled with ceramic beads to trap submicron particles, thus facilitating detailed analysis of the fluidized medium.

The fluidization of air within the system is precisely controlled and monitored using rotameters from CT Platon, enabling accurate measurement of gas flow rates. The bed height at the onset of each experiment is carefully set to approximately 20 mm above the distributor plate's flange, ensuring consistency in experimental conditions. The critical task of determining the minimum fluidization velocity involves detailed assessments of pressure drops, starting from a port above the distributor plate. Experimental procedures within this setup include the strategic manipulation of two distinct particle types classified under Geldart's grouping. These procedures entail varying the superficial gas velocities to cover the full scale of the rotameters, alongside detailed measurements of pressure drops and thorough X-ray analyses.

The employed X-ray system offers a non-invasive method for obtaining both qualitative and quantitative insights into the reactor's internal dynamics and the instantaneous behaviour of the fluidized bed in three dimensions [33]. Utilizing a pulsed, high-energy X-ray beam, the system captures changes in attenuation resulting from the interactions between solids and fluids within the reactor. The detection of these X-rays is facilitated by a 30 cm Industrial X-ray Image Intensifier paired with a high-speed camera, which captures images at 50 frames per second [34]. This sophisticated setup allows for the meticulous measurement of pressure drop profiles at varying gas velocities, with air serving as the fluidizing medium and its flow rate regulated by a precisely calibrated rotameter.

The experimental protocol was carried out under controlled laboratory conditions, maintaining standard ambient temperature and pressure, with air serving as the principal fluidizing medium. The flow

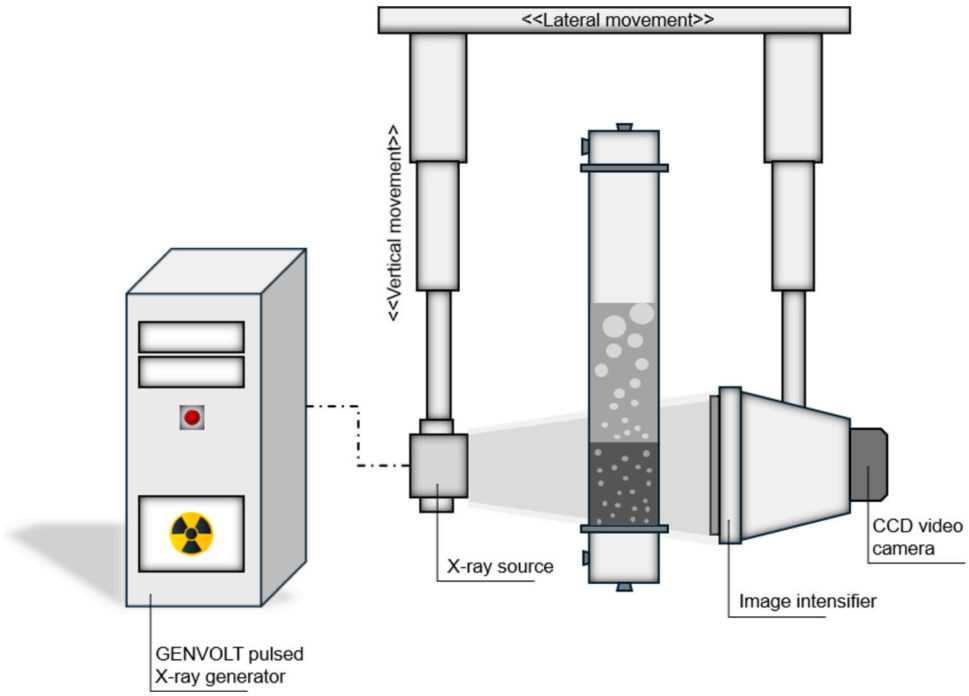

Fig. 1. Scheme of the X-ray system unit.

rate of air was meticulously adjusted using a calibrated rotameter to ensure precise control over the fluidizing process. In assessing the pressure drop across the bed, the procedure involved incrementally increasing the velocity of the gas until the particles within the bed were optimally fluidized. Following this, the flow rate was methodically reduced until the particles settled back into a non-fluidized state. To guarantee the reliability and reproducibility of the results, these measurements were performed multiple times, typically ranging from three to five iterations.

The experimental design incorporated the use of two distinct types of mixed powder, namely FCC (Fluid Catalytic Cracking catalyst) and Rutile (TiO_2), to simulate different materials commonly used in industrial processes. FCC, categorized as a Geldart group A particle, was selected to mimic transferable materials such as adsorbents or zeolitic substances, due to its comparable properties in terms of particle size and density. Conversely, Rutile, identified as a Geldart group B particle, was chosen to represent metal catalysts typically utilized in dual bed systems (e.g., Cu/ZnO or Fe_2O_3), attributed to its larger particle size and higher density, mirroring those of metal catalysts. Considering Glicksman's scaling rules, we also maintained a reasonable ratio of ρ_s/ρ_g (solid density to gas density), D_c/d_p (column diameter to particle diameter), u_0/u_{mf}, sphericity, particle size distribution for both types of particles, ensuring resemblance to the exemplary case of syngas-to-olefins vie methanol synthesis [17,35,36]. This careful adherence to scaling laws is crucial for accurately simulating the behaviour of fluidized beds in industrial processes, thereby enhancing the reliability and efficiency of scale-up operations. The experimental approach involved establishing the minimum fluidization velocity for FCC, thereby providing a baseline for comparison. Following this, the minimum fluidization velocity for Rutile was also determined. This methodology facilitated a direct comparison between the fluidization behaviours of the two different materials, yielding critical insights into their respective dynamic responses and operational efficacies within the dual bed system. The measured density of FCC and rutile is 800 and 2800 kg/m^3, respectively. Table 1 shows the physical properties of the experimental materials, along with a comparison to related published works under real operating conditions.

For each set of experiments focusing on the distinct particle groups, a detailed investigation was undertaken to examine various volume ratios of FCC and rutile particles, as carefully documented in Table 2. In other published studies on binary particle systems, the volume ratio of catalyst to absorbent varied, such as 0.23:0.3 (NiO to CaO) [37], 1:1 (Cu/ZnO/Al_2O_3 to hydrotalcite) [5], 3:7 (Cu/ZnO/Al_2O_3 to zeolite) [38]. Based on these studies, we selected a reasonable range of volume ratios for our experiments. The experimental methodology necessitated a thorough blending of the two particle types to achieve a homogeneous mixture. This carefully curated mixture was then strategically layered within the reactor to ensure an even distribution of both particle groups. The intentional layering process was designed to establish an optimal and homogeneous arrangement, aiming for a balanced distribution of the

Table 2
Experimental matrix for binary particle fluidization test.

Mixture	1	2	3	4	5
FCC (A)	95 vol%	85 vol%	75 vol%	65 vol%	55 vol%
Rutile (B)	5 vol%	15 vol%	25 vol%	35 vol%	45 vol%

Table 1
Physical properties of the experimental materials and comparison with published works for methanol synthesis and methanol-to-olefins.

Binary mixture (A; B)	Gas and condition	Avg. particle size (micron)	ρ_s/ρ_g	D_c/d_p	Sphericity	h/D_c	u_0/u_{mf}
FCC; Rutile	Air (20 °C, 1 bar)	60; 200	650; 2300	470; 140	0.8	17.8	1–26
Zeolite; Cu-ZnO/Al_2O_3 [17,35,36]	Syngas (220–280 °C, 5–30 bar)	90; 300	100–650; 400–2400	100–800; 80–320	0.8–1	10–27	2–10

two distinct particle types across the reactor system from the outset. The primary objective of these experiments was to conduct an in-depth analysis of the mixing and segregation patterns that emerge within the fluidized bed reactor. By exploring a range of volume ratios, the experiments aimed to unravel the complex dynamics of particle interaction and segregation within the reactor's dynamic environment. This methodical approach allowed for a deeper understanding of the unique behaviours and interactions between the FCC and rutile particles within the fluidized bed system.

Multiple definitions of an axial mixing index or segregation index for binary mixtures have been proposed. The segregation index usually varies between zero and one, with zero indicating no segregation or uniform mixing and one indicating a completely segregated mixture. By comparing the average grayscale and brightness distribution of X-ray images at different positions, we can determine the mixing ratio of the two particles at these positions.

It should be noted that the minimum fluidization velocity for each component of a binary mixture can be accurately estimated using well-known Ergun-type correlations for individual particles, such as the Wen and Yu equation [39]. Numerous studies have examined various models to determine the minimum fluidization velocity in binary mixtures of solid particles. Among these models, Cheung equation is commonly used to compute the overall minimum fluidization velocity for binary particle mixtures [31]:

$$U_{mf} = U_F(U_J/U_F)^{x_P^2} \tag{1}$$

Fu et al. proposed a correlation based on the Cheung equation by introducing an adjustable parameter. This method has been reported to be a superior approach for estimating the minimum fluidization velocity of binary mixtures of solid particle [32]:

$$U_{mf} = U_F(U_J/U_F)^{x_P^{1.26\times(d_J/d_F)^{-0.53}}} \tag{2}$$

In our research, we use adapted Gibilaro-Rowe (GR) model to analyze the segregation patterns we observed experimentally [26]. The original GR model outlines three mixing mechanisms—identified as the rates of solid circulation (w), material exchange (q), and axial mixing (r)—alongside a single segregation mechanism, denoted as the segregation rate (k). There is an assumption that no mixing or segregation occurs horizontally, and that the values of w, q, and k do not vary with changes in bed height. Differential equations are applied to describe the movement of jetsam in both the wake and bulk phases of the bed, focusing on the balance within a thin slice of the bed with thickness dz.

$$\frac{dC_B}{dz}(w+k-2kC_B)+qH(C_w-C_B)=0 \tag{3}$$

$$w\frac{dC_w}{dz}-qH(C_B-C_w)=0 \tag{4}$$

In the model, C_B and C_W represent the volumetric fractions of jetsam in the bulk and wake phases of the bed, respectively. Here, z denotes the normalized height, while H is the total height of the bed. The average concentration of jetsam throughout the bed (C_{ave}) can be determined based on the fraction of solids present in the wake phase (F_w). This calculation is essential for understanding the distribution of jetsam within the fluidized bed and for analysing its segregation dynamics:

$$C_{ave} = F_wC_W-(1-F_w)C_B \tag{5}$$

A dimensionless number, λ, has been employed to correlate the circulation rate (w) with the segregation rate (k), expressed as λ = w/k [26]. This parameter serves as an indicator of the segregation propensity within the solid mixture. Consequently, higher values of λ suggest a reduced tendency for segregation, indicating greater solid circulation rates and lower segregation rates, and the reverse is true for lower values of λ. The parameters F_w, w, q, and k can be calculated from the correlations [40]:

$$F_W = \frac{a_B'F_{WB}}{1-a_B} \tag{6}$$

$$w = u_bF_{WB}\left(\frac{a_B'}{1-a_B'}\right) \tag{7}$$

$$q = 1.5\frac{F_{WB}u_{mf}}{d_B\epsilon_{mf}}\left(\frac{a_B'}{1-a_B'}\right) \tag{8}$$

$$k = \frac{3}{4}\overline{Y}_su_b\left(\frac{a_B'}{1-a_B'}\right) \tag{9}$$

Bubble rise velocity [41]:

$$u_b = (u_0-u_{mf})+0.711\sqrt{gd_b} \tag{10}$$

volume fraction of the wake in the bubble [40]:

$$F_{WB} = \frac{1}{2}-\frac{9}{16}cos\left(\frac{\theta_W}{2}\right)+\frac{1}{16}cos\left(\frac{3\theta_W}{2}\right) \tag{11}$$

wake angle [24]:

$$\theta_W = 160-160e^{(-60d_b)} \tag{12}$$

volume fraction of wakes and bubbles in the bed [40]:

$$a_B' = \frac{u_0-u_{mf}}{u_b(1-F_{WB})} \tag{13}$$

volume fraction of bubbles in the bed [40]:

$$a_B = (1-F_{WB})a_B' \tag{14}$$

dimensionless segregation distance [42]:

$$\overline{Y}_s = 0.6\left(\frac{\rho_J}{\rho_F}\right)\left(\frac{d_J}{d_F}\right)^{1/3} \tag{15}$$

$$\overline{Y}_s = 0.8\left(\frac{\rho_J}{\rho_{bulk}}\right)\left(\frac{d_J}{d_{bulk}}\right)^{1/3}-0.8 \tag{16}$$

$$\overline{Y}_s = 0.8\left[\frac{d_J\rho_J^{1/3}}{(1-\overline{C_{ave}})\rho_Fd_F^{1/3}+\overline{C_{ave}}\rho_Jd_J^{1/3}}-1\right] \tag{17}$$

3. Results and discussion

3.1. Minimum fluidization velocity of binary mixtures

The bed pressure drop versus superficial gas velocity curve was used to determine the minimum fluidization velocity. Binary mixtures of FCC and rutile particles with different particle compositions and densities were tested, and the corresponding pressure-drop and air flow velocity curves of the binary mixtures are shown in Fig. 2. The minimum fluidization velocity is determined experimentally by plotting the pressure drop against gas velocity. It is identified at the intersection of two lines: one showing the increasing pressure drop as gas velocity rises, and the other representing the constant pressure drop once the bed is fully fluidized. Compared with the single particle system, the binary system exhibits additional features such as incipient and total fluidization velocities. Among these fluidization velocities, the minimum fluidization velocity is particularly important for characterizing a binary system, especially for the modelling and design of fluidized bed operations.

Table 3 shows the comparison of minimum fluidization velocities of binary mixtures from equation calculations and experiments. It is evident that the modified equation of Fu et al. [32] demonstrated a better match across different mixing ratios of binary particles. The solid particles used in this experiment belong to Geldart Group A/B particles.

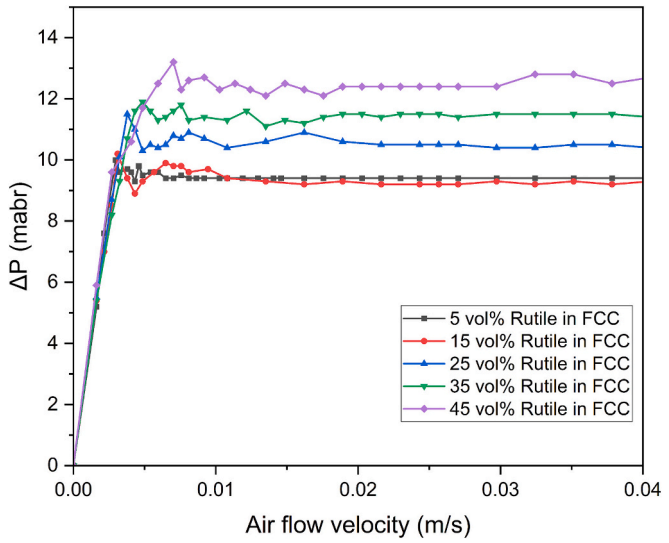

Fig. 2. Pressure-drop and air flow velocity curve of the binary mixtures.

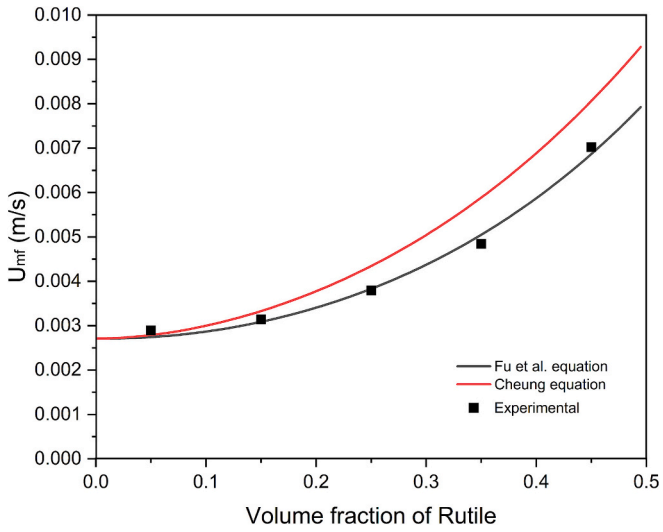

Fig. 3. Minimum fluidization velocity curve of binary mixtures from equation calculation.

Table 3
Minimum fluidization velocities of binary mixtures from equation calculation and experiments (unit: m/s).

	Mixture 1	Mixture 2	Mixture 3	Mixture 4	Mixture 5
Experimental	0.00289	0.00314	0.00379	0.00484	0.00702
Cheung	0.00278	0.00333	0.00434	0.00588	0.00806
Fu et al.	0.00274	0.00308	0.00383	0.00505	0.00686

The results indicate a relationship between the minimum fluidization velocity and the volume fraction of binary particles in the mixtures. When the system contains only 5 vol% rutile, the minimum fluidization velocity of the mixtures remains nearly unchanged compared to the original value for FCC. However, when the volume fraction of rutile exceeds 5 vol%, the minimum fluidization velocity of the mixtures varies significantly, approaching the minimum fluidization velocity of rutile. This behaviour can be attributed to the partial fluidization and bed voidage variation in binary systems at the minimum fluidization state.

According to the modified equation by Fu et al. (Eq. 2), the particle size ratio is a fundamental parameter for characterizing a binary mixture and can be easily derived from the properties of the solid particles. As shown in Fig. 3, the modified equation provides a better match for predicting minimum fluidization velocities. Additionally, empirical correlations offer the advantage of being simple and reasonably accurate for specific experimental data sets. For design and operational purposes, it is essential to calculate the minimum fluidization velocity of binary mixtures of medium particles to avoid the need for extensive experimental measurements. The modified equation by Fu et al. is recommended as a reliable method for estimating the minimum fluidization velocity of binary mixtures of solid particles. By incorporating the particle size ratio (d_p/d_f), this approach improves predictive accuracy, offering a more effective means of analysing binary systems. It could also be further investigated to predict the segregation and mixing behaviours of binary particle systems in fluidized beds.

3.2. *Effect of binary mixture composition on fluidization behaviour*

Based on the minimum fluidization velocities of binary mixtures and pressure drop results, we employed the X-ray imaging system to investigate the fluidization behaviours of the binary particles and compare the experimental results with the calculated segregation curve. The effect of air flow velocities on the segregation profiles with binary particles at different mixing ratios (rutile: 15, 25, 35, and 45 vol%) is represented in Fig. 4. Since 5 vol% of rutile in FCC did not produce clear images or distinguishable mixing/segregation patterns, it is not included in the figure. The X-ray images on the left illustrate the segregation and mixing behaviours of binary particle mixtures at various air flow velocities. These images provide a visual representation of how different flow rates impact the distribution and interaction of particles within the fluidized bed. On the right, Fig. 4 presents a comparative analysis between the experimental results and the modelling predictions of average jetsam particle concentrations along the bed. The figures illustrate the axial concentration profiles for various mixtures containing different fractions of jetsam. This comparison is made at three representative air flow velocities: 0.00542, 0.0163, 0.0303 m/s, which correspond to 2, 6, and 12 times the minimum fluidization velocities of FCC particles. These specific velocities were chosen to demonstrate the range of behaviours observed under different conditions, highlighting how changes in air flow influence the degree of segregation and mixing in the system.

A similar phenomenon was observed at different mixing ratios, with the behaviour of the lighter FCC materials particularly notable. These materials exhibited significant segregation capabilities at elevated flow rates, leading to a marked expansion within the fluidized bed. Once the gas velocity exceeded 0.054 m/s— about 20 times the minimum fluidization velocity of FCC—elutriation of FCC particles occurred, which is undesirable for reactor operation as it indicates excessive particle carryover. The initiation of particle segregation was observed at different velocities for varying compositions of group B particles. Specifically, segregation began at 0.0092 m/s for 15 vol% rutile, 0.0097 m/s for 25 vol% rutile, 0.0102 m/s for 35 vol% rutile, and 0.0108 m/s for 45 vol% rutile. As the gas velocities increased beyond these initial points, the segregation phenomenon became increasingly pronounced. This was evident through the distinct separation of particle layers and the enhanced movement of the lighter FCC particles to the upper regions of the bed, while the denser rutile particles settled below. The critical height (z*) that demarcates the zones enriched in jetsam and flotsam slightly decreases, and the concentration of jetsam in the upper region of the bed rises at higher gas velocities. At low flow rates, the particles remain stationary until the gas reaches a critical velocity, causing the mixture to become fluidized.

At even higher gas flow rates, the particle bed undergoes complete segregation into horizontal layers, as illustrated in Fig. 4. A distinct phase of complete segregation was observed within specific velocity ranges: 0.0189 to 0.0338 m/s for 15 vol% rutile, 0.0195 to 0.0345 m/s for 25 vol% rutile, 0.0230 to 0.0345 m/s for 35 vol% rutile, and 0.0244

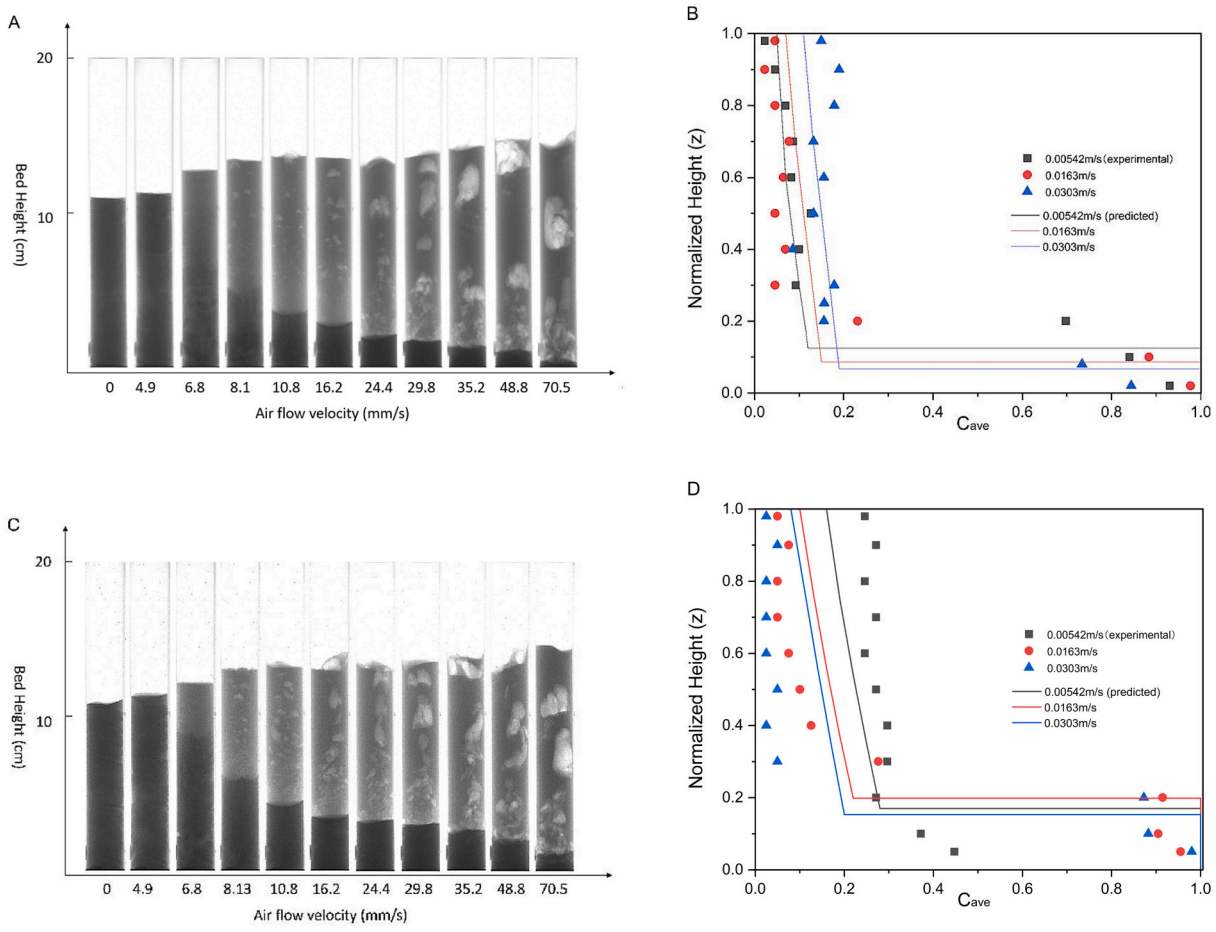

Fig. 4. Expansion curves and pressure drop profile for the full range of velocities tested. Coloured dots are the experimental results, the coloured lines are corresponding simulation curve using modified GR model. A, C, E, G: X-ray images of Mixture 2, 3, 4, 5 at different air flow velocities, respectively. B, D, F, H: Experimental results and model predictions for Mixture 2, 3, 4, 5 at different air flow velocities, respectively.

to 0.0365 m/s for 45 vol% rutile. This progression of segregation patterns over various gas flow rates demonstrates that within these ranges, the growth rate of the bottom layer remains almost constant regardless of the gas velocity. This constancy indicates that the segregation process is independent of the convective movement in the mixed layer above the coarse particle layer.

The predicted curve also showed a good match with the experimental results. Within a certain range, increasing air flow velocity led to improved segregation behaviour, with 0.0303 m/s exhibiting better segregation than 0.0163 m/s, which in turn was better than 0.00542 m/s. This indicates that higher air flow velocities within this range enhance the segregation of particles, aligning well with the model's predictions and the observed experimental outcomes.

Small bubbles initially appear within the jetsam layer due to localized fluidization of the heavier particles. These bubbles, formed by the upward flow of gas, provide pathways for the gas to travel through the dense jetsam layer. As these bubbles rise through the bed, they encounter the less dense flotsam layer above. In this transition, the bubbles merge and coalesce, resulting in larger bubbles within the flotsam layer. The increase in bubble size is facilitated by the lower resistance and higher mobility of the lighter flotsam particles, which allow the gas bubbles to expand and merge more easily.

Following this phase of complete segregation, a re-mixing of the particles was observed as the velocity increased further. This re-mixing phase indicates the dynamic nature of the fluidized bed environment, where, under specific conditions, the initially segregated particles can reintegrate. This phenomenon demonstrates the intricate interplay of forces and particle characteristics within the bed. Additionally, the model provides a satisfactory prediction of jetsam concentration, especially for experiments with relatively lower rutile ratios (15 and 25 vol %). Notably, other models often fail or do not accurately predict segregation patterns in mixtures with high jetsam concentrations [42,43]. However, the modified model, applied with the modified Cheung equation, exhibited considerable potential for further application. It allows for predicting the segregation and mixing behaviour of binary particle systems in fluidized beds without requiring extensive experimentation.

Fig. 5 illustrates the mechanism of segregation behaviour as gas velocity increases. Initially, the two types of particles are fully mixed at the beginning of the experiment. As the gas flow velocity gradually increases, a critical point is reached where the flotsam particles in the upper region of the bed begin to fluidize, forming an expanding layer. Concurrently, the jetsam particles establish a stable layer beneath. Upon further increase in flow rate, the bed remains distinctly segregated into two layers, with both layers eventually exhibiting fluidization. Small bubbles appear within the jetsam layer, which subsequently merge into larger bubbles in the flotsam layer. It is only at very high velocities that bubble-induced mixing becomes prominent, leading to the intermixing of the two phases.

The fluidization mechanism governing the behaviour of a binary mixture of solid particles is notably more complex than that of systems with monodisperse particles. This complexity is evident across a wide

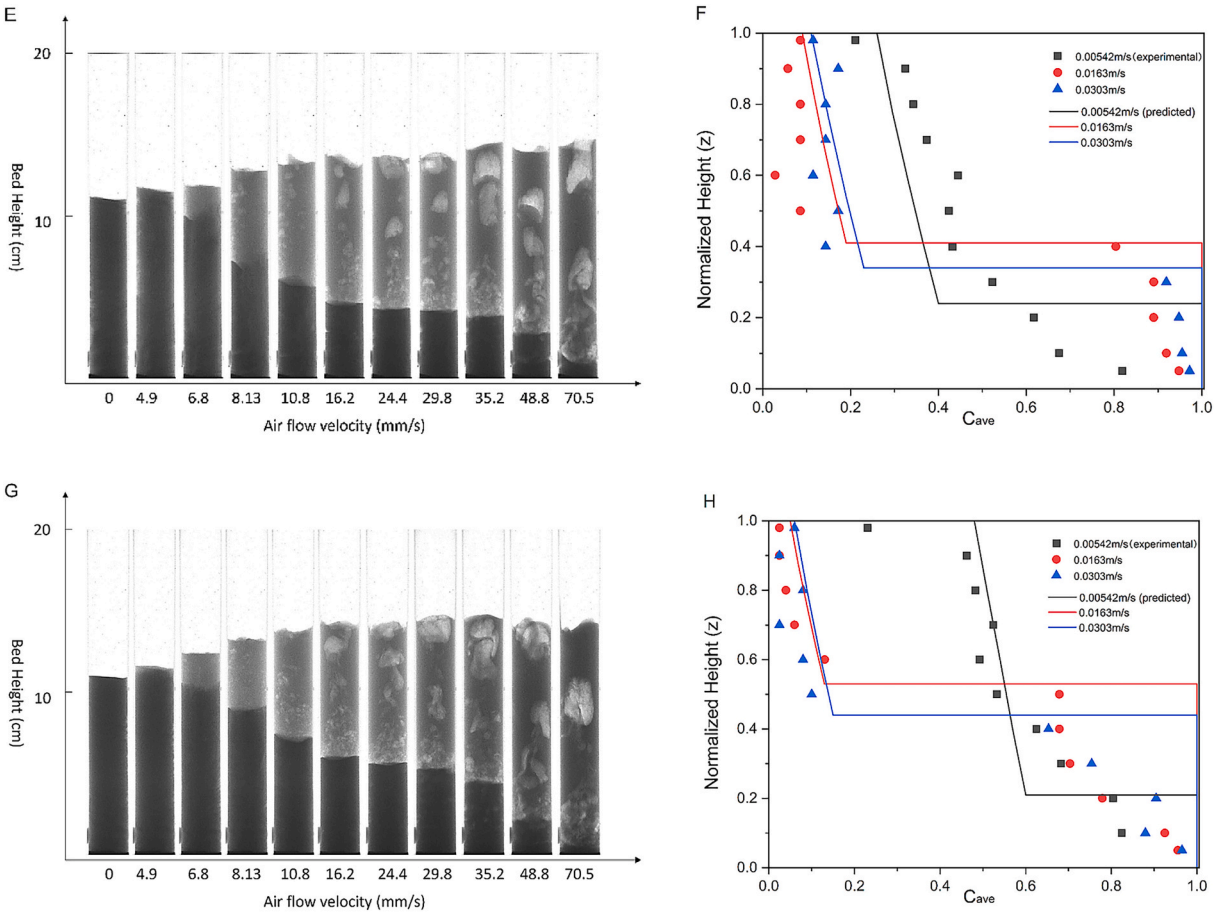

Fig. 4. (*continued*).

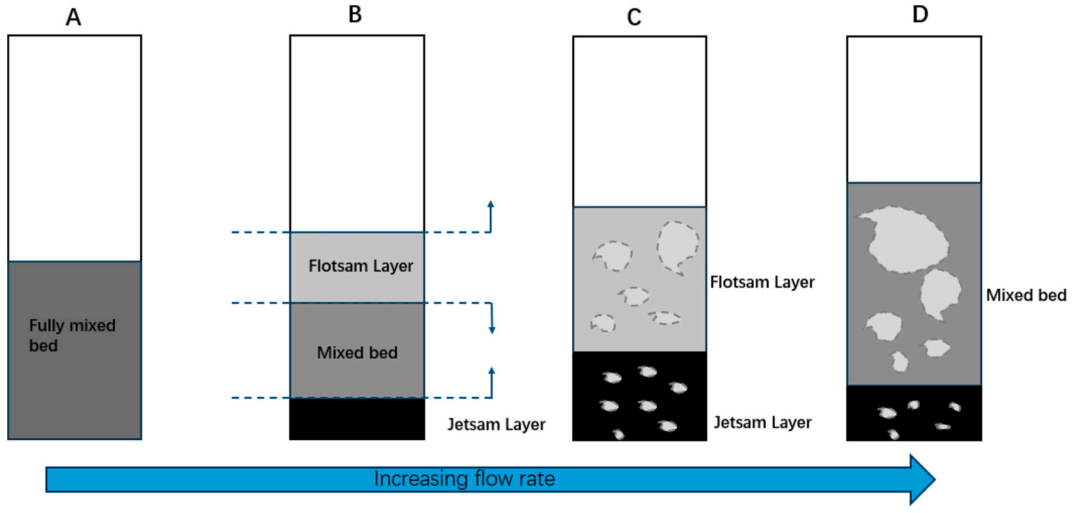

Fig. 5. Schematic of bed behaviour at increasing gas velocity. A: initial fully mixed bed; B: partially segregated bed; C: ideally segregated bed; D: partially mixed bed.

range of gas velocities, involving processes of simultaneous segregation and remixing of the particles. The schematic representation in Fig. 5 provides a visual understanding of these phenomena, highlighting the intricate dynamics of segregation and mixing within the fluidized bed.

In the realm of fluid dynamics, especially within the context of fluidized beds containing free-flowing particles classified under Geldart Groups A and B, a unique pattern of behaviour emerges as gas velocity is methodically increased. Initially, within the static bed configuration, particles are distributed in a relatively uniform manner. However, as gas velocity approaches a critical threshold, a dynamic shift occurs, signaling the onset of fluidization. This critical juncture is characterized by the upward movement of Group A particles, which are typically lighter and smaller, forming a thin, yet expansive fluidized layer at the upper region of the bed. This initial fluidization phase is marked by the formation of a pseudo-fluidic state, wherein these lighter particles exhibit fluid-like behaviour.

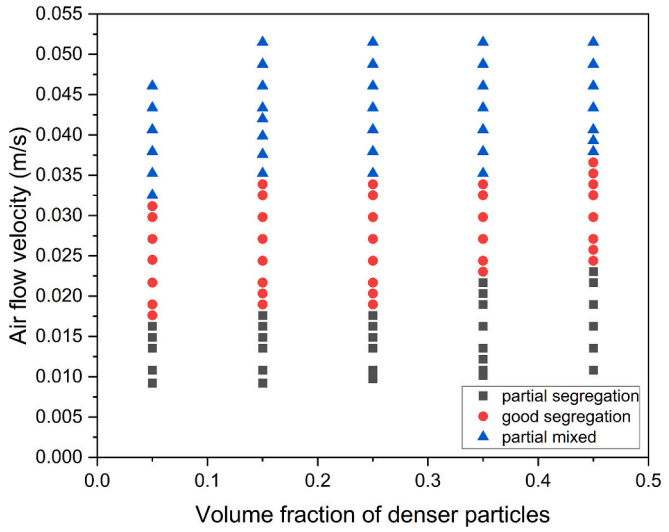

Fig. 6. Phase diagrams for the mixtures of particles based on experimental observations. The different symbols correspond to the distinct structures observed. Partial segregation: the major volume of the bed is segregated. Partial mixed: the major volume of the bed is mixed.

Beneath this active layer, a denser arrangement of Group B particles, which are inherently larger and heavier, forms a distinct, static layer. Initially, these heavier particles are interspersed among the lighter particles, but as fluidization commences, they segregate due to the differential in drag forces exerted by the upward-flowing gas.

As gas velocity continues to escalate within a designated range, the bed maintains its segregated state, characterized by the coexistence of two stratified layers. This period of segregation is critical for certain industrial applications where differentiation between particle types is desired. Examples include the extraction of zeolite particles for regeneration in oil refining units, and the extraction of one solid adsorbent phase for regeneration in dual bed systems. Additionally, there is potential for utilizing freely circulating fluidized beds (CFBs) to enhance the efficiency of particle separation and regeneration processes. By understanding and optimizing these parameters, the design and operation of fluidized bed systems can be significantly improved, leading to enhanced performance and efficiency in various industrial applications [44]. Subsequently, as fluidization intensifies, both the flotsam and jetsam layers begin to display signs of fluidization. Notably, within the jetsam layer, small bubbles emerge due to the localized fluidization of Group B particles. These bubbles coalesce and ascend into the flotsam layer, where they grow in size and contribute to the layer's expansion.

Fig. 6 shows the phase diagrams for the mixtures of particles based on experimental observations. The regimes identified are described as incipient motion, where particles begin to move but have not yet segregated; partial segregation, where rutile particles start to accumulate at the bottom of the bed; good segregation, characterized by clear separation of rutile and FCC particles into distinct layers; and partial mixing, where some degree of mixing occurs between the particles. The diagrams illustrate that increasing the volume percent of rutile raises the initial air flow velocity required to reach both the partial segregation zone and the good segregation zone. This indicates that higher concentrations of group B particles necessitate higher gas velocities to achieve similar segregation. Additionally, it is observed that mixtures with 15 vol% and 25 vol% rutile exhibit comparable good segregation zones in terms of the air flow velocities needed. From 0.0244 to 0.0311 m/s, all five different rutile volumes are in the good segregation zone, suggesting that adjusting the ratio of binary particles can achieve similar

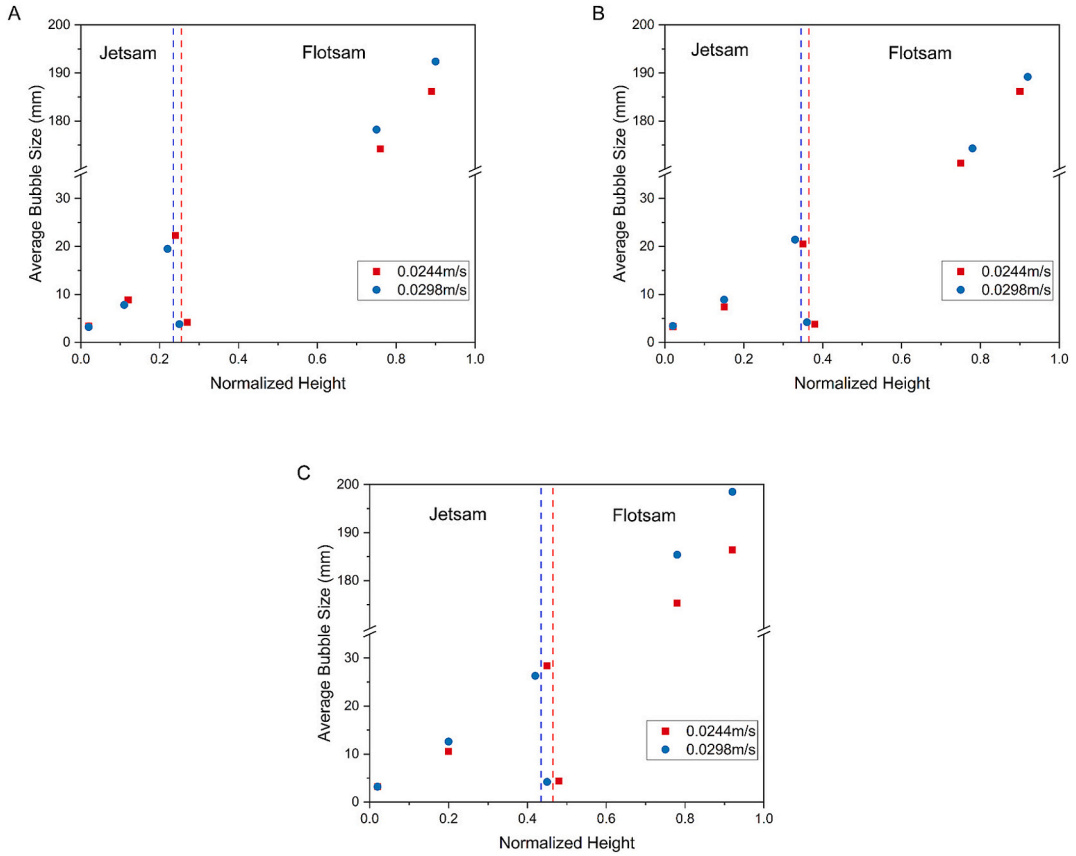

Fig. 7. Effect of different jetsam (rutile) particle ratios and superficial gas velocities on average bubble diameter at different heights (A: Mixture 3, B: Mixture 4, C: Mixture 5).

segregation behaviour at comparable air flow rates. This observation is consistent with the simulated results in Fig. 4, where the simulation curve at an air flow rate of 0.0298 and 0.0303 m/s shows clear segregation at different mixing ratios. This indicates that the model can predict segregation and mixing patterns under certain conditions. Furthermore, experiments conducted at various mixing ratios demonstrated consistent structures and behaviours across different conditions. These results, obtained from experiments performed in a cylindrical container and using an X-ray imaging system, provided detailed observations of the bed's interior. Compared to other studies using thin pseudo-2D fluidized beds, our findings suggest that the observed segregation behaviour is not dependent on planar geometry and is likely inherent to the particle mixtures themselves.

Fig. 7 illustrates the effect of varying particle ratios of jetsam (25 %, 35 %, 45 % rutile) on the evolution of bubble size at different heights within the bed, under two different air flow velocities (0.0244 m/s and 0.0298 m/s). As expected, increasing the gas velocity leads to the formation of larger bubbles, which facilitates the transfer of excess air to the bed surface. The behaviour of bubbles differs significantly between the jetsam (Group B) and flotsam (Group A) layers. Bubbles at the bottom of the jetsam layer are initially of similar size but grow larger as they ascend. At the interface between the jetsam and flotsam layers, bubbles broke up, and divided into multiple smaller bubbles above the interface. Furthermore, as the flotsam layer increases in length the average bubble diameter in this layer becomes larger, indicating the progressive coalescence of bubbles rising through Group A materials, which are known for slower bubble velocities and more uniform fluidization [45]. These observations are consistent with the literature on the behaviour of Geldart Group A and B particles in fluidized systems, where bubble size, growth, and dynamics are strongly influenced by particle properties and bed composition [45–47]. Notably, by breaking up bubbles at an intermediate height, the interphase between the two solid phases acts like an internal baffle, thus improving gas-solid distribution, and reducing gas by-pass associated to large bubbles [48].

4. Conclusions

The functioning parameters of a multi-functional system delineate a specific velocity range that enables the bed to uphold a state of segregation while simultaneously allowing for the fluidization of both jetsam and flotsam elements. Intriguingly, despite this state of segregation, observable distinctions in the fluidization behaviours of the two layers emerge. By employing a combination of a modified Cheung equation to determine the minimum fluidization velocity of a binary particle system and a modified version of the model proposed by Gibilaro and Rowe, this paper investigates the segregation behaviours of mixtures of Geldart Group A and B materials at different mixing rates and air flow velocities. The results showed a good match between the experimental data and the predictions of the modified models. Additionally, it has been shown that a bed consisting of a mixture of particles of different sizes can have a variety of different structures depending on the gas flow rate through it, segregation can persist when the gas flow rate is sufficiently large. Under such conditions it can be shown that the segregation behaviour can be successfully modelled, providing a comprehensive analysis of the interactions between different particle types under varied conditions. The potential impact of this work is significant for both experimental and industrial applications. By simplifying the prediction and modelling of mixing and segregation behaviour, it becomes easier to enhance efficiency and performance in reactor and process design. Specifically, the research can help addressing critical factors such as the optimal location of the extraction point, the selection of appropriate superficial gas velocities, and the determination of suitable particle sizes. These improvements can lead to enhanced processes in multifunctional catalytic systems and sorption enhanced catalytic processes, accelerating deployment in industrial context.

List of symbols

a_B	volume fraction of wakes and bubbles in the bed
C_{ave}	average volumetric fraction of jetsam
C_B	volumetric fraction of jetsam in the bulk phase
C_W	volumetric fraction of jetsam in the wake phase
d	particle diameter (m)
d_b	bubble diameter (m)
F_w	volume fraction of solid in the wake
F_{WB}	volume fraction of the wake in the bubble
H	total bed height (m)
k	segregation coefficient (m/s)
q	exchange rate coefficient (s^{-1})
u	velocity (m/s)
w	solids circulation rate (m/s)
x_J	mass fraction of the jetsam (−)
Y_s	dimensionless segregation distance
z	normalized height

Greek letters

Δp	bed pressure drop (MPa)
ϵ	bed voidage
ρ	density (kg/m^3)

Subscript

0	fluidizing gas
b	bubble
bulk	bulk
F	flotsam
J	jetsam
mf	minimum fluidization conditions of the mixture
p	component with the highest minimum fluidization velocity

CRediT authorship contribution statement

Hualun Zhu: Writing – review & editing, Writing – original draft, Investigation, Data curation. **Paola Lettieri:** Writing – review & editing, Resources. **Massimiliano Materazzi:** Writing – review & editing, Resources, Project administration, Funding acquisition, Conceptualization.

Declaration of competing interest

The authors declare that they have no known competing financial interests or personal relationships that could have appeared to influence the work reported in this paper.

Acknowledgements

The authors gratefully acknowledge the financial support from the Engineering and Physical Sciences Research Council (EPSRC) through the "Nature-inspired bio-Syngas Technologies for Olefins Synthesis" Grant (EP/W019221/1).

Data availability

Data will be made available on request.

References

[1] Z. Luo, et al., Recent advances on the uses of biomass alternative fuels in cement manufacturing process: a review, Energy Fuel 38 (9) (2024) 7454–7479.
[2] R.A. Cocco, J.W. Chew, Fluidized Bed Scale-up for Sustainability Challenges. 1. Tomorrow's Tools, Industrial & Engineering Chemistry Research, 2024.
[3] M. Materazzi, M. Materazzi, Gasification of waste derived fuels in fluidized beds: Fundamental aspects and industrial challenges, in: Clean Energy from Waste:

Fundamental Investigations on Ashes and Tar Behaviours in a Two Stage Fluid Bed-Plasma Process for Waste Gasification, 2017, pp. 19–63.
[4] A. Coppola, et al., Evaluation of two sorbents for the sorption-enhanced methanation in a dual fluidized bed system, Biomass Convers. Biorefinery 11 (2021) 111–119.
[5] Y. Ju, et al., Performance and dynamic behavior of sorption-enhanced water-gas shift reaction in a fluidized bed reactor for H2 production and CO2 capture, Chem. Eng. J. 410 (2021) 127414.
[6] H.V. Ly, et al., Catalytic pyrolysis of spent coffee waste for upgrading sustainable bio-oil in a bubbling fluidized-bed reactor: experimental and techno-economic analysis, Chem. Eng. J. 427 (2022) 130956.
[7] B. Zhang, et al., Oil shale upgrading by gas-solid high density separation fluidized bed under secondary accumulation distribution, Fuel 262 (2020) 116468.
[8] A. Lyngfelt, et al., Achieving adequate circulation in chemical looping combustion—design proposal for a 200 mwth chemical looping combustion circulating fluidized bed boiler, Energy Fuel 36 (17) (2022) 9588–9615.
[9] I. Gogolev, et al., Investigation of biomass alkali release in a dual circulating fluidized bed chemical looping combustion system, Fuel 297 (2021) 120743.
[10] F. Parrillo, et al., Fluidized bed gasification of eucalyptus chips: axial profiles of syngas composition in a pilot scale reactor, Energy 219 (2021) 119604.
[11] B. Leckner, F. Lind, Combustion of municipal solid waste in fluidized bed or on grate–a comparison, Waste Manag. 109 (2020) 94–108.
[12] F. Winter, B. Schratzer, 23 - applications of fluidized bed technology in processes other than combustion and gasification, in: F. Scala (Ed.), Fluidized Bed Technologies for Near-Zero Emission Combustion and Gasification, Woodhead Publishing, 2013, pp. 1005–1033.
[13] S. Parvathaneni, V.V. Buwa, Role of bubbling behaviour in segregation and mixing of binary gas-solids flow of particles with different density, Powder Technol. 372 (2020) 178–191.
[14] G.A. Tafete, N.G. Habtu, Reactor configuration, operations and structural catalyst design in process intensification of catalytic reactors: a review, Chem. Eng. Process. Process Intensif. 184 (2023) 109290.
[15] S. Bhaskaran, S. Gupta, S. De, Dual fluidized bed gasification of solid fuels, in: Coal and Biomass Gasification: Recent Advances and Future Challenges, 2018, pp. 425–454.
[16] Y. Wang, Y. Li, Sorption-enhanced steam gasification of biomass for H2-rich gas production and in-situ CO2 capture by CaO-based sorbents: a critical review, Appl. Energy Combust. Sci. 14 (2023) 100124.
[17] A. Coppola, et al., Evaluation of two sorbents for the sorption-enhanced methanation in a dual fluidized bed system, Biomass Convers. Biorefinery 11 (1) (2021) 111–119.
[18] D.C. Guío-Pérez, T. Pröll, H. Hofbauer, Solids residence time distribution in the secondary reactor of a dual circulating fluidized bed system, Chem. Eng. Sci. 104 (2013) 269–284.
[19] J. Krūmiņš, M. Kļaviņš, Integrated circulating fluidized bed gasification system for sustainable municipal solid waste management: energy production and heat recovery, Energies 16 (13) (2023) 5203.
[20] L. Yassin, et al., Techno-economic performance of energy-from-waste fluidized bed combustion and gasification processes in the UK context, Chem. Eng. J. 146 (3) (2009) 315–327.
[21] J. Grace, G. Sun, Influence of particle size distribution on the performance of fluidized bed reactors, Can. J. Chem. Eng. 69 (5) (1991) 1126–1134.
[22] F. Alamolhoda, et al., Effect of changes in particle size on the hydrodynamics of gas-solid fluidized beds through wall vibration, Powder Technol. 307 (2017) 129–136.
[23] Z. Wang, M. Kwauk, H. Li, Fluidization of fine particles, Chem. Eng. Sci. 53 (3) (1998) 377–395.
[24] A. Hoffmann, L. Janssen, J. Prins, Particle segregation in fluidised binary mixtures, Chem. Eng. Sci. 48 (9) (1993) 1583–1592.
[25] P. Tang, V. Puri, Methods for minimizing segregation: a review, Part. Sci. Technol. 22 (4) (2004) 321–337.
[26] L.G. Gibilaro, P. Rowe, A model for a segregating gas fluidised bed, Chem. Eng. Sci. 29 (6) (1974) 1403–1412.
[27] S. Geng, et al., CFD modeling the hydrodynamics of binary particle mixture in pseudo-2D bubbling fluidized bed: effect of model parameters, Powder Technol. 302 (2016) 384–395.
[28] H. Ma, Y. Zhao, CFD-DEM investigation of the fluidization of binary mixtures containing rod-like particles and spherical particles in a fluidized bed, Powder Technol. 336 (2018) 533–545.
[29] R.K. Reddy, J.B. Joshi, CFD modeling of solid–liquid fluidized beds of mono and binary particle mixtures, Chem. Eng. Sci. 64 (16) (2009) 3641–3658.
[30] S. Turrado, J.R. Fernández, J.C. Abanades, Investigation of the segregation of binary mixtures with Iron-based particles in a bubbling fluidized bed, ACS Omega 4 (5) (2019) 9065–9073.
[31] L. Cheung, Minimum fluidisation velocity of a binary mixture of different sized particles, Chem. Eng. Sci. 29 (5) (1974) 1301–1303.
[32] Z. Fu, et al., Minimum fluidization velocity of binary mixtures of medium particles in the air dense medium fluidized bed, Chem. Eng. Sci. 207 (2019) 194–201.
[33] M. Errigo, et al., Application of imaging techniques for the characterization of lumps behaviour in gas–solid fluidized-bed reactors, Fuel 349 (2023) 128634.
[34] L. Panariello, et al., X-ray imaging of horizontal jets in gas fluidised bed nozzles, Chem. Eng. Sci. 164 (2017) 53–62.
[35] S. Ledakowicz, et al., Kinetic characterisation of catalysts for methanol synthesis, Chem. Process. Eng. 4 (2013).
[36] M.E.E. Abashar, A.A. Al-Rabiah, Investigation of the efficiency of sorption-enhanced methanol synthesis process in circulating fast fluidized bed reactors, Fuel Process. Technol. 179 (2018) 387–398.
[37] S. Yang, et al., Investigation of sorption-enhanced hydrogen production by glycerol steam reforming in bubbling fluidized bed, Fuel 349 (2023) 128731.
[38] M. Menéndez, et al., A preliminary assessment of sorption-enhanced methanol synthesis in a fluidized bed reactor with selective addition/removal of the sorbent, Catalysts 14 (7) (2024) 409.
[39] C. Wen, Y. Yu, A generalized method for predicting the minimum fluidization velocity, AICHE J. 12 (3) (1966) 610–612.
[40] N. Naimer, T. Chiba, A. Nienow, Parameter estimation for a solids mixing| segregation model for gas fluidised beds, Chem. Eng. Sci. 37 (7) (1982) 1047–1057.
[41] D. Nicklin, Two-phase bubble flow, Chem. Eng. Sci. 17 (9) (1962) 693–702.
[42] H. Tanimoto, et al., Jetsam descent induced by a single bubble passage in three-dimensional gas-fluidized beds, J. Chem. Eng. Jpn 14 (4) (1981) 273–276.
[43] A.C. Hoffmann, E.J. Romp, Segregation in a fluidised powder of a continuous size distribution, Powder Technol. 66 (2) (1991) 119–126.
[44] R. Singh, E. Gbordzoe, Modeling FCC spent catalyst regeneration with computational fluid dynamics, Powder Technol. 316 (2017) 560–568.
[45] X. Zhu, et al., Mixing/segregation characteristics and bubble behaviors of density-segregated binary particles in a pressurized fluidized bed, Powder Technol. 434 (2024) 119367.
[46] M. Zarepour, et al., Largest Lyapunov exponent and Shannon entropy: two indices to analyze mixing in fluidized beds, Chem. Eng. Res. Des. 210 (2024) 59–70.
[47] A. Busciglio, et al., Experimental analysis of bubble size distributions in 2D gas fluidized beds, Chem. Eng. Sci. 65 (16) (2010) 4782–4791.
[48] H.S. Rennebaum, et al., The effect of baffles on the hydrodynamics of a gas-solid fluidized bed studied using real-time magnetic resonance imaging, Powder Technol. 432 (2024) 119114.